CdS@SiO_2 Core–Shell Electroluminescent Nanorod Arrays Based on a Metal–Insulator–Semiconductor Structure

Chunfeng Wang, Dengfeng Peng, Jing Zhao, Rongrong Bao, Tianfeng Li, Li Tian, Lin Dong, Changyu Shen,* and Caofeng Pan**

***E**normous advancement has been achieved in the field of one-dimensional (1D) semiconductor light-emitting devices (LEDs), however, LEDs based on 1D CdS nanostructures have been rarely reported. The fabrication of CdS@SiO_2 core–shell nanorod array LEDs based on a Au–SiO_2–CdS metal–insulator–semiconductor (MIS) structure is presented. The MIS LEDs exhibit strong yellow emission with a low threshold voltage of 2.7 V. Electroluminescence with a broad emission ranging from 450 nm to 800 nm and a shoulder peak at 700 nm is observed, which is related to the defects and surface states of the CdS nanorods. The influence of the SiO_2 shell thickness on the electroluminescence intensity is systematically investigated. The devices have a high light-emitting spatial resolution of 1.5 μm and maintain an excellent emission property even after shelving at room temperature for at least three months. Moreover, the fabrication process is simple and cost effective and the MIS device could be fabricated on a flexible substrate, which holds great potential for application as a flexible light source. This prototype is expected to open up a new route towards the development of large-scale light-emitting devices with excellent attributes, such as high resolution, low cost, and good stability.*

C. Wang, J. Zhao, L. Tian, Prof. C. Shen
Engineering Research Center for Advanced Polymer Processing Technology
School of Materials Science and Engineering
Zhengzhou University
100 Science Avenue, Zhengzhou 450001, P. R. China
E-mail: shency@zzu.edu.cn

C. Wang, Dr. D. Peng, J. Zhao, Dr. R. Bao, Dr. T. Li, Prof. L. Dong, Prof. C. Pan
Beijing Institute of Nanoenergy and Nanosystems
Chinese Academy of Science
National Center for Nanoscience and Technology (NCNST)
Beijing 100083, P. R. China
E-mail: ldong@zzu.edu.cn; cfpan@binn.cas.cn

Prof. L. Dong
School of Physical Engineering
Zhengzhou University
100 Science Avenue, Zhengzhou 450001, P. R. China

DOI: 10.1002/smll.201601548

1. Introduction

One-dimensional (1D) semiconductor nanostructures have attracted intensive investigation because of their potential applications for a wide variety of optoelectronics, ranging from solar cells, light-emitting devices (LEDs), to lasers and photodetectors.[1–5] As for LEDs, nanorods (NRs) or nanowires (NWs) provide exciting advantages compared to their film-based counterparts. Firstly, the NR or NW geometry enables strain relaxation through the NR or NW sidewalls thus facilitating the dislocation-free epitaxy of highly lattice-mismatched materials.[6,7] Secondly, NRs or NWs contain natural waveguiding cavities, which are expected to be an effective approach for improving the extraction efficiency of as-fabricated LEDs.[7,8] Thirdly, NRs or NWs can be fabricated in the form of crossover arrays, which offers the possibility of combining different luminescent materials to achieve integrated polychromatic emission.[9] Fourthly, the

inherent shape anisotropy of NRs or NWs can provide additional benefits, such as polarized light emission.[10–12] Because of the above-mentioned advantages, GaN-based LEDs (e.g., $In_xGa_{1-x}N/Al_xGa_{1-x}N$ core–shell and axial heterojunction structures) and ZnO-based LEDs (e.g., p–n homojunction and n-ZnO/p-GaN heterojunction structures) have been extensively studied as UV–visible light sources.[13–15] However, the sophisticated and expensive fabrication methods needed for GaN-based LEDs and the lack of consistent p-type ZnO structures have retarded their development for further applications. As a II–VI type semiconductor, CdS has a very similar structure and physical properties as those of ZnO and GaN and a more favorable bandgap of 2.54 eV for visible emission, which can play an important role in nanoscale electronic and optoelectronic devices.[16] Unfortunately, electroluminescent devices based on 1D CdS nanostructures have thus far been rarely reported, except for Huang et al., who fabricated a single CdS nanowire light-emitting diode by crossing a CdS nanowire with a p-Si nanowire,[17] and Duan et al., who reported an electronically driven laser of a CdS single nanowire based on a $Au/Al_2O_3/CdS/p^+$-Si structure.[18] These limited reports may be due to the problems that are associated with the aligned and large-scale growth of CdS NR or NW arrays. Moreover, electroluminescent devices at the level of a single nanowire usually result in a low quantum efficiency due to the small effective emission area. Thus, it is important to fabricate electroluminescent devices based on large-scale CdS NR or NW arrays toward practical applications.

Here, we demonstrate the first large-scale light-emitting device based on a Au–SiO_2–CdS metal–insulator–semiconductor (MIS) structure consisting of a CdS@SiO_2 core–shell NR array. The MIS structure is greatly beneficial for LEDs, as it provides unique carrier-recombination physics, instead of using p-type semiconductors, and it provides an excellent structural stability.[19,20] We adopted core–shell tactics so as to significantly suppress the surface non-radiative recombination of the LEDs and avoid the quantum-confined Stark effect.[21–23] The CdS@SiO_2 core–shell NR array was prepared by combining a low-temperature hydrothermal method with plasma-enhanced chemical vapor deposition (PECVD). The MIS LEDs exhibited a strong yellow emission with a low threshold voltage of 2.7 V, and maintained an excellent emission property, even after leaving them in the open air for at least three months without any encapsulation. The electroluminescent (EL) spectrum showed a broad-band emission ranging from 450 nm to 800 nm with a shoulder peak at 700 nm, which can be attributed to various defects and surface states of the CdS by deconvoluting the EL spectrum with Gaussian functions. An approximate light-emitting spatial resolution of 1.5 μm was found, as defined by the full-width at half-maximum (FWHM) of the line profile of the emission intensity. This high resolution will be beneficial to achieve high pixel densities in imaging systems. The thickness of the SiO_2 shell layer was found to have an important effect on the emission intensity of the LEDs and we systematically investigated and optimized it to achieve the best light-emitting performance of the device. We fabricated a flexible MIS device to show the potential of this prototype as a flexible light source. The excellent properties and simple fabrication process of the device pave the way to cost-effective and large-scale light-emitting devices based on 1D CdS nanostructures.

2. Results and Discussion

The schematic fabrication process of the MIS LEDs is illustrated in **Figure 1**a. A CdS NR array was firstly grown on a pre-cleaned fluorine-doped tin oxide (FTO) glass substrate via a hydrothermal process[24] (see details in the Experimental Section). Subsequently, a SiO_2 thin film was deposited via PECVD as the shell to cover the CdS NRs. The thickness of the shell could be adjusted by appropriate tuning of the deposition time. Then, poly(methyl methacrylate) (PMMA) was spin-coated to wrap the core–shell NRs and O_2 reactive ion etching (RIE) was applied to expose the heads of the core–shell NRs. Finally, a layer of Au (30 nm) was deposited as the top electrode via electron-beam evaporation (e-beam). The top-view (Figure 1b) and cross-sectional (Figure 1c) scanning electron microscopy (SEM) images show that the CdS NRs were hexagonal in shape with an average diameter of 180 nm and length of 600 nm. The vertical CdS NRs sit on top of a dense buffer layer that covers the FTO substrate. Figure 1d shows an SEM image of the CdS@SiO_2 core–shell NRs after PMMA spin-coating and O_2 etching, showing that the heads of the NRs are exposed after etching, leaving the main body and bottom of the NRs still completely wrapped, which greatly ameliorates the robustness of the device. Figure 1e shows the X-ray diffraction (XRD) pattern of the CdS NRs grown on FTO glass, indicating their wurtzite crystal phase. The dominant (002) peak indicates the high crystalline quality of the CdS NRs and its prioritized orientation along the *c*-axis.

The CdS@SiO_2 core–shell structure was further characterized by transmission electron microscopy (TEM). The deposition time of the SiO_2 shell via PECVD was 80 s. **Figure 2**a shows a TEM image of a typical CdS@SiO_2 core–shell nanorod, in which both top and sidewalls of the CdS nanorod were coated with the SiO_2 shell. The shell thickness at the top was much thicker than that of the sidewalls owing to the shadow effect among neighboring NRs,[25] which resulted in a non-uniform shell thickness that decreased gradually from the top to the bottom along the NR. The selected area-electron diffraction (SAED) pattern in Figure 2b demonstrates an obvious single-crystal structure of the CdS nanorod with matched well with the (002) and $(2\,\bar{1}\,0)$ planes. From the high-resolution TEM (HRTEM) image in Figure 2c (derived from the selected area marked in Figure 2a), the high quality of the crystalline structure of the CdS NR can be observed and a plane spacing of 0.67 nm along the *c*-axis can be seen, as well as a well-defined interface of the CdS@SiO_2 core–shell. The elemental mapping images were obtained by energy-dispersive X-ray spectroscopy (EDS), as shown in Figure 2d–g, further identifying the core–shell structure.

The electroluminescence performance of a representative MIS LED was carefully studied, whereby the deposition time of the SiO_2 shell was 80 s. The current–voltage

DOI: 10.1002/smll.201601548

small NANO MICRO

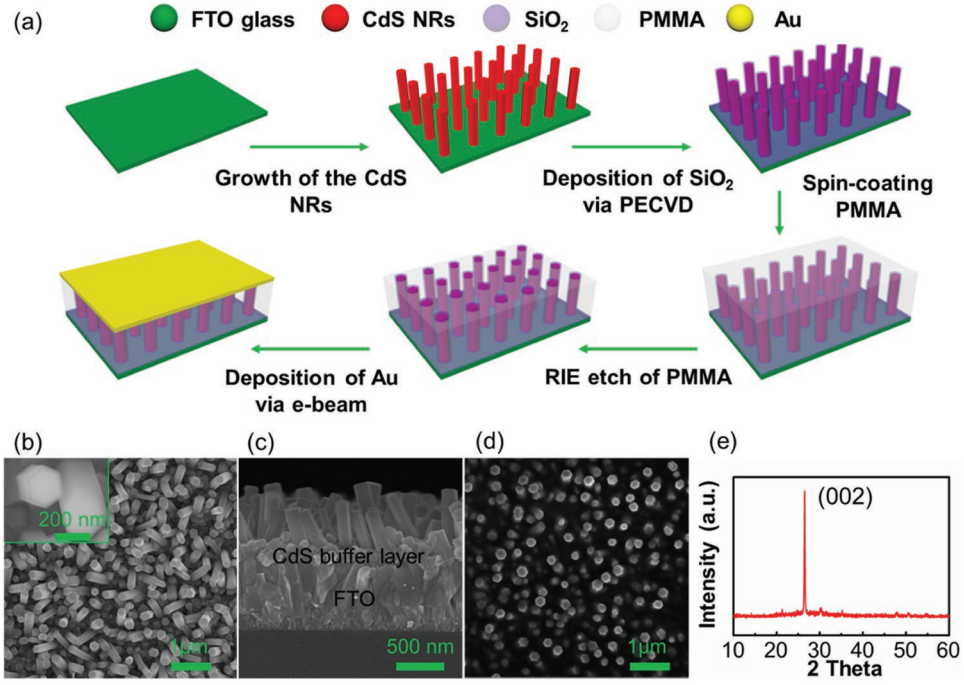

Figure 1. Fabrication of the MIS LEDs: a) Schematic illustration of the MIS LED fabrication process. b) SEM image of the CdS nanorods. The inset shows an enlarged view of the nanorod with a diameter of 180 nm. c) Cross-sectional SEM image of the CdS nanorods, showing an average length of 600 nm. d) SEM image of the CdS@SiO_2 core–shell nanorods with exposed tips after spin-coating of PMMA and O_2 reactive ion etching. e) XRD pattern of the CdS nanorods on the FTO glass.

(*I*–*V*) characteristics of the device are presented in **Figure 3**a, showing a low threshold voltage of 2.7 V. The inset in Figure 3a illustrates the operation of the device, where the negative voltage is connected to the FTO glass. The wavelength-dependent electroluminescent spectra of the device at different bias between 3 and 9 V are shown in Figure 3b, from which a broad defect-related emission ranging from 450 nm to 800 nm with a shoulder peak at 700 nm can be observed. The emission mechanism of the device will be explained in detail in a subsequent section. A photograph of the emission of a device with a top Au electrode pattern reading "CdS" is shown in Figure 3c. The devices mainly generated a yellow emission visible to the naked eye above the threshold voltage, and maintained an excellent emission even after being shelved at room temperature and ambient air for at least three months without any encapsulation, proving its

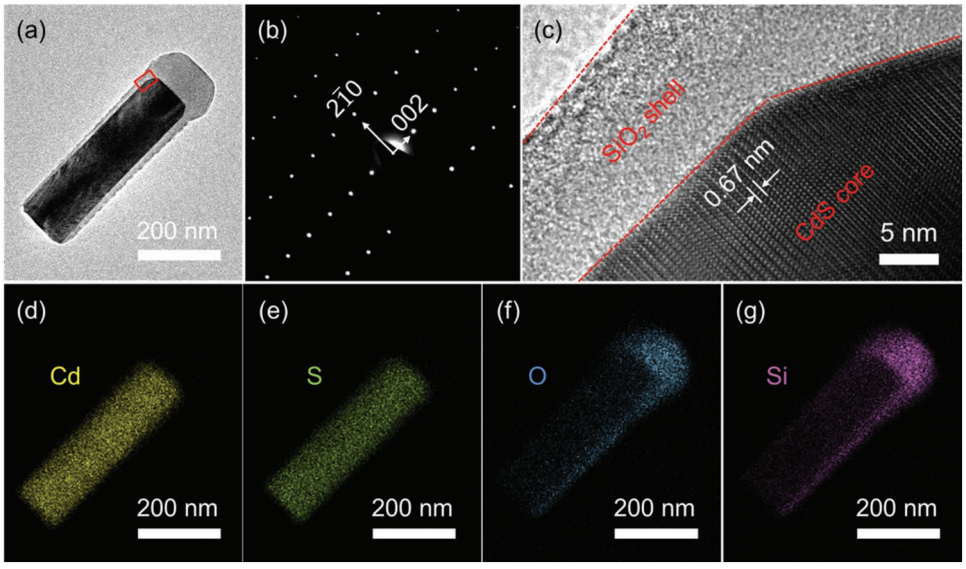

Figure 2. Characterization of the CdS@SiO_2 core–shell structure: a) TEM image of a typical CdS@SiO_2 core–shell nanorod. b) SAED pattern from the core–shell nanorod body. c) HRTEM image of the core–shell nanorod, showing the interface between CdS core and SiO_2 shell. d–g) Energy dispersive X-ray spectroscopy (EDS) images of the core–shell nanorod showing the elemental distribution of Cd, S, O, and Si, respectively.

DOI: 10.1002/smll.201601548

www.MaterialsViews.com

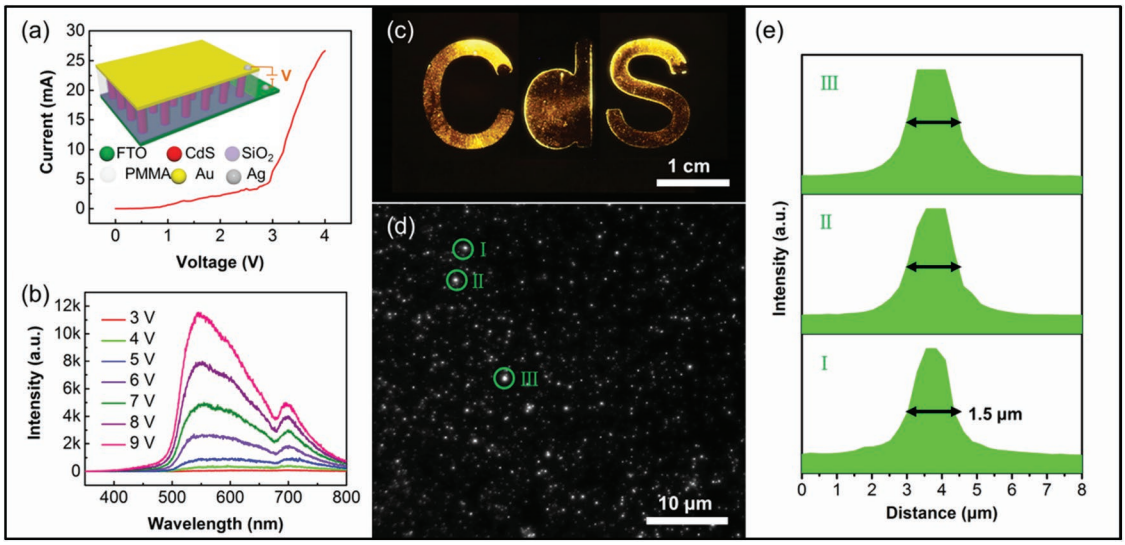

Figure 3. Electroluminescence of the MIS LEDs: a) *I–V* characteristics of the device. The inset represents the demonstration device, where the negative voltage is connected to the FTO glass. b) EL spectra of the device at different bias voltages in the range of 3–9 V. c,d) Photograph and optical microscopy image of representative devices. e) Line profile of the emission intensity from three spots marked in Figure d, in which the light-emitting spatial resolution of the device can be estimated.

good stability. Figure 3d shows the optical microscopy images of the working device and Figure 3e shows the corresponding line profiles of the emission intensity from the three marked spots in Figure 3d. From this we obtained a light-emitting spatial resolution of about 1.5 μm as defined by the FWHM of the emission intensity.[26] The high spatial resolution of the device will be beneficial to achieve high pixel densities in imaging systems.

To elucidate the emission mechanism, a schematic band diagram of the device is presented in **Figure 4**a. When a bias is applied to the device, electron injection occurs through the FTO glass substrate. However, a large amount of electrons will be confined in the downwards-bent region of the conduction band of the CdS NR because of the considerably high energy barrier of SiO_2. The accumulated electrons are necessary to generate EL emission. In the case of hole

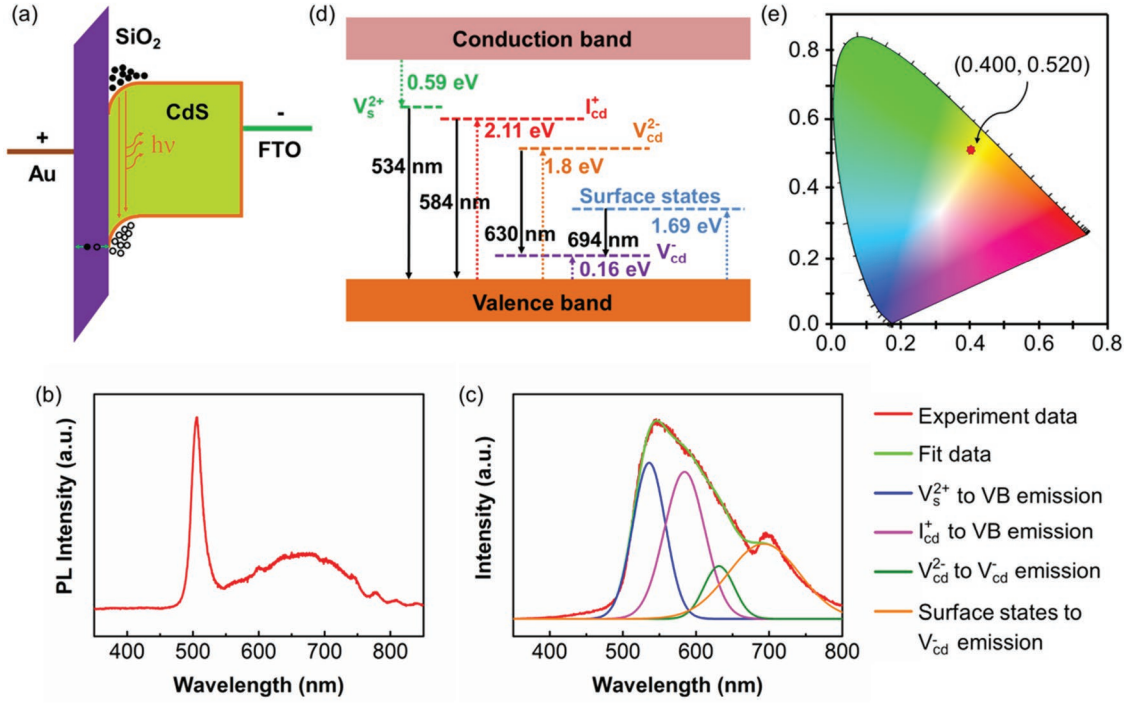

Figure 4. Emission mechanism of the MIS LEDs: a) Schematic band diagram of the MIS structure. b) PL spectrum of the as-grown CdS nanorods. c) Peak deconvolution of the EL spectrum with Gaussian functions at the bias of 9 V. d) Schematic energy level diagram to illustrate the origins of the recombination luminescence. e) CIE chromaticity diagram of the light-emitting device for the EL spectrum at 9 V.

small 2016,
DOI: 10.1002/smll.201601548

injection, electron–hole pairs are first generated in the SiO_2 layer through impact ionization created by the high electric field under sufficient bias.[27] Then the electron–hole pairs separate and the holes are swept into the valence-band region of the CdS NR by the bias. The defect-related emission may be attributed to the high defect concentration of the CdS NR synthesized via the low-temperature solution process,[28] as identified by the photoluminescence (PL) spectrum of the as-grown CdS NRs in Figure 4b, showing a near-band-edge emission and a broad defect-related emission. To better understand the physical process of the light emission, we conducted a peak deconvolution of the EL spectrum with Gaussian functions, which is shown in Figure 4c, indicating that the EL emission includes four defect-related peaks located at 534 nm, 584 nm, 630 nm, and 694 nm. The origins of the four peaks were carefully studied and are schematically illustrated in Figure 4d. There are five defect-related energy levels in CdS except for the valence band (VB) and conduction band (CB) that may contribute to the electroluminescence:[29] a positive divalent sulfur vacancy (V_S^{2+}) donor level located at 0.59 eV below the CB,[30] a positive univalent cadmium interstitial donor level (I_{Cd}^{+}) located at 2.11 eV above the VB,[31] a bi-negative cadmium vacancy (V_{Cd}^{2-}) level located at 1.80 eV above the VB,[32] a negative univalent cadmium vacancy (V_{Cd}^{-}) acceptor level located at 0.16 eV above the VB,[33] and surface states at 1.69 eV above the VB.[34] The four emission peaks can be explained as follows: i) The green emission at 534 nm can be ascribed to the radiative transition of V_S^{2+} to the VB; ii) the yellow emission at 584 nm can be ascribed to the transitions of I_{Cd}^{+} to the VB; iii) the orange emission at 630 nm can be assigned to the recombination of V_{Cd}^{2-} to V_{Cd}^{-}; iv) the red emission at 694 nm originated from the transitions from the surface states to V_{Cd}^{-}. Figure 4e shows the Commission International d'Eclairage (CIE) chromaticity diagram of the device with the EL spectrum at 9 V. The calculated color coordinates were (0.400, 0.520), which were very close to those of the yellow light (0.479, 0.520).

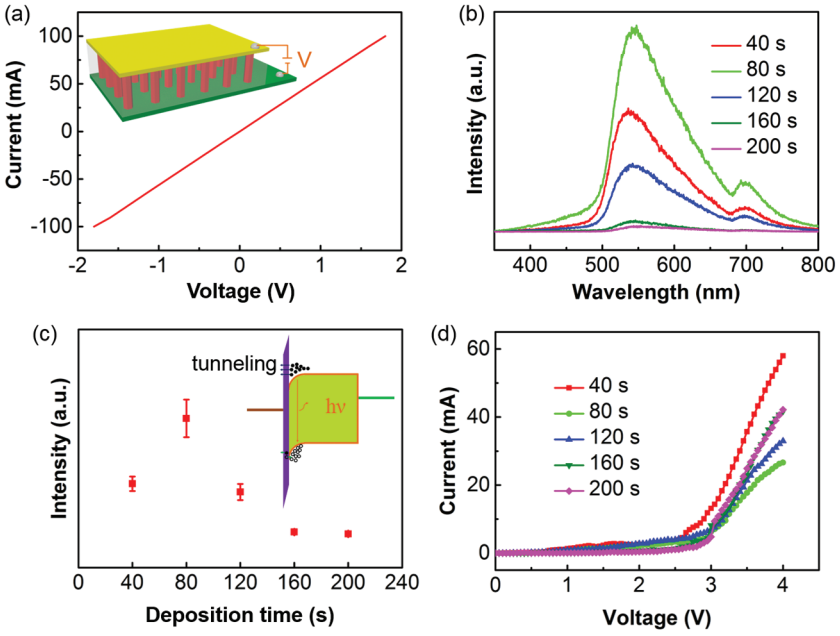

Figure 5. Effect of the thicknesses of the SiO_2 shell layer on the emission performance of the MIS LEDs. a) *I–V* behavior of a device without SiO_2 layer. b) EL spectra of the as-fabricated devices with different deposition times of the SiO_2 shell (200 s, 160 s, 120 s, 80 s, and 40 s). c) Dependence of the light-emitting intensity at the peak position of 550 nm on the deposition time of the SiO_2 shell. d) *I–V* curves of the as-fabricated devices with different deposition times of the SiO_2 shell.

The SiO_2 shell layer played an important role in our device. There was no light detected from devices without SiO_2 shell and their *I–V* characteristics exhibited an ohmic behavior, as shown by **Figure 5**a, indicating that the SiO_2 shell is essential for the light emission. We also investigated the effect of the thickness of the SiO_2 shell on the emission performance of the device. The shell thickness depended on the PECVD deposition time and we therefore used the deposition time as a variable to induce a non-uniformity in the shell. Figure 5b shows the EL spectra of as-fabricated devices with different deposition times of the SiO_2 shell, namely 200 s, 160 s, 120 s, 80 s, and 40 s. The emission intensity of the device increased with decreasing deposition time except that the intensity of the 40-s device is lower than for the 80-s device. This can be explained more intuitively by the dependence of the emission intensity at the peak position of 550 nm on the deposition time of SiO_2, as shown in Figure 5c. The reason might be related to the reduced series resistance with decreasing thickness of the SiO_2 shell, leading to an improved emission efficiency. But when the thickness keeps decreasing and falls below a certain value, electron tunneling occurs through the narrow SiO_2 layer, thus lowering the emission efficiency. This phenomenon was confirmed by the *I–V* characterizations of the devices, as shown in Figure 5d. The current of the devices dropped with decreasing deposition time under the same bias, indicating the improved recombination of electrons and holes. The abnormal current of the device with the 40-s deposition time can be explained by the electron-tunneling effect.

The development of flexible light-emitting devices has been the subject of much recent research because of their great applications in flexible displays and wearable electronics. Here, we demonstrate a flexible light-emitting device based on the Au–SiO_2–CdS MIS structure. The schematic illustration of our flexible device is shown in **Figure 6**a. A Kapton film was used as the substrate, on which Cr and Au were deposited by magnetron sputtering as the adhesive layer and bottom electrode, respectively. The fabrication process was similar to that of the rigid device based on the FTO glass substrate. Figure 6b and 6c represent the digital photograph and the corresponding emission image of the flexible device, proving the feasibility of the Au–SiO_2–CdS MIS structure for flexible light sources.

DOI: 10.1002/smll.201601548

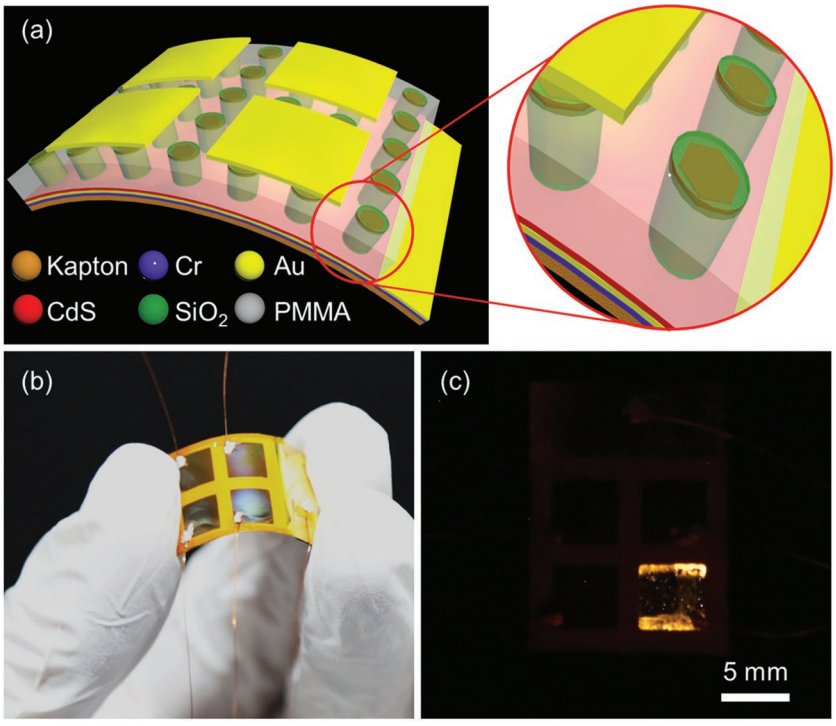

Figure 6. A flexible LED based on the CdS@SiO_2/Au MIS structure: a) Schematic illustration of the flexible MIS light-emitting device. b) Digital photograph of the flexible device. c) Optical image of the flexible device when electronically lit up.

3. Conclusion

We have for the first time fabricated a large-scale light-emitting device utilizing a CdS@SiO_2 core–shell nanorod array based on an MIS structure. The MIS structure and core–shell tactics endow the device with excellent stability and optoelectronic properties with a strong yellow emission above the threshold voltage of 2.7 V. The SiO_2 shell thickness was systematically investigated and optimized to achieve an optimal emitting intensity. The light-emitting mechanism was explained in detail by a schematic band diagram. The simple fabrication process of the device can easily be upscaled for large-scale production. As compared to single-nanowire devices, the large scale LED has a much larger effective active region, and accordingly a higher light-emitting efficiency. Furthermore, the MIS device can work on a flexible substrate, although this still deserves further study, showing its potential applications in flexible displays and portable electronics. This work represents one step towards practical applications of nano-LEDs through the use of 1D CdS nanostructures, and is expected to attract more attention for the development of 1D CdS LEDs.

4. Experimental Section

4.1. Hydrothermal Synthesis of the CdS Nanorod Array

The CdS nanorod array was prepared on fluorine-doped tin oxide (FTO) glass by a hydrothermal process as described previously.[24] First, a nutrient solution of 15 mM was obtained by mixing thiourea, cadmium nitrate, and reduced glutathione at a molar ratio of 1:1:0.6 in deionized water, which was then put into a stainless steel autoclave. Subsequently, the pre-cleaned FTO glass was put into the autoclave with its growth surface facing down. Then the autoclave was sealed and kept in an oven at 200 °C for 8 h for CdS nanorod array growth. The obtained sample was rinsed with deionized water for several times and dried at 70 °C for 5 h.

4.2. Assembly of the Au-SiO_2-CdS MIS Light-Emitting Device

After growth of the CdS nanorod array, a thin layer of SiO_2 was deposited via plasma-enhanced chemical vapor deposition (PECVD) as the shell to cover the CdS nanorods. The chamber pressure was 1 Pa with flow rates of SiH_4, O_2, and Ar of 130.5, 13, and 126 sccm, respectively. The excitation power and substrate temperature were 450 W and 80 °C, respectively. The thickness of the shell could be controlled by changing the deposition time, ranging from 40 s to 200 s. Then, poly(methyl methacrylate) (PMMA) was spin-coated to wrap the core–shell nanorods and O_2 reactive ion etching (RIE) was applied to expose the tips of the nanorods. Lastly, a layer of Au (30 nm) was deposited via electron-beam evaporation (e-beam) as the top electrode. A similar fabrication process was used for the flexible MIS light-emitting device except that the substrate was Kapton/Cr/Au, in which the Cr (10 nm) and Au (50 nm) were deposited via magnetron sputtering as the adhesive layer and bottom electrode, respectively.

4.3. Characterization

The morphology of the CdS nanorod array was characterized by scanning electron microscopy (SEM, FEI Nova NanoSEM 450). XRD patterns were acquired using an X-ray diffractometer (PANalytical X'Pert 3 Powder) with a Cu Kα radiation source. The photoluminescence (PL) spectra were obtained using a confocal micro-Raman spectroscope (Horiba Jobin-Yvon LabRAM HR Evolution) with a He:Cd laser (Kimmon IK3301R-G) of 5 mW at 325 nm. The transmission electron microscopy (TEM) images and energy-dispersive X-ray spectroscopy (EDS) mapping were collected by a FEI Tecnai G2 F20 S-TWIN TMP equipped with an EDAX (Materials Analysis Division, Apollo XLT2). The current–voltage (I–V) curves of the device were recorded using a Keithley 4200 SCS. The electroluminescence (EL) spectra were collected using a fluorescence spectrometer (EI FLS980-S2S2-stm). Optical microscopy images were recorded using a Zeiss Observer Z1 inverted microscope equipped with an HQ2 camera.

Acknowledgements

The authors are thankful for the support from the "Thousand Talents" program of China for pioneering researchers and innovative

DOI: 10.1002/smll.201601548

teams and from the President Funding of the Chinese Academy of Sciences, National Natural Science Foundation of China (No. 51272238, 51432005, 61405040, 61505010, 51502018, and U1404619), the Beijing City Committee of Science and Technology (Z151100003315010), the Beijing Natural Science Foundation (2164077 and 2164076), the Talent Project of Zhengzhou University (ZDGD13001), and the Surface Engineering Key Lab of LIPCAST. We thank Prof. Xiangyang Ma at Zhejiang University for his generous assistance and helpful discussion.

[1] H. Li, X. Wang, J. Xu, Q. Zhang, Y. Bando, D. Golberg, Y. Ma, T. Zhai, *Adv. Mater.* **2013**, *25*, 3017.
[2] Z. Fan, L. Xiaohua, P. Caofeng, Z. Jing, *Nanotechnology* **2007**, *18*, 345302.
[3] L. Dong, S. Niu, C. Pan, R. Yu, Y. Zhang, Z. L. Wang, *Adv. Mater.* **2012**, *24*, 5470.
[4] W. Guo, C. Xu, G. Zhu, C. Pan, C. Lin, Z. L. Wang, *Nano Energy* **2012**, *1*, 176.
[5] C. Pan, Z. Luo, C. Xu, J. Luo, R. Liang, G. Zhu, W. Wu, W. Guo, X. Yan, J. Xu, Z. L. Wang, J. Zhu, *ACS Nano* **2011**, *5*, 6629.
[6] A. T. M. G. Sarwar, S. D. Carnevale, F. Yang, T. F. Kent, J. J. Jamison, D. W. McComb, R. C. Myers, *Small* **2015**, *11*, 5402.
[7] A. B. Wong, M. Lai, S. W. Eaton, Y. Yu, E. Lin, L. Dou, A. Fu, P. Yang, *Nano Lett.* **2015**, *15*, 5519.
[8] X. Li, J. Qi, Q. Zhang, Q. Wang, F. Yi, Z. Wang, Y. Zhang, *Appl. Phys. Lett.* **2013**, *102*, 221103.
[9] J. Zhu, Y. Cui, *Small* **2007**, *3*, 1322.
[10] N. Oh, S. Nam, Y. Zhai, K. Deshpande, P. Trefonas, M. Shim, *Nat. Commun.* **2014**, *5*, 3642.
[11] S. Nam, N. Oh, Y. Zhai, M. Shim, *ACS Nano* **2015**, *9*, 878.
[12] D. van Dam, D. R. Abujetas, R. Paniagua-Domínguez, J. A. Sánchez-Gil, E. P. A. M. Bakkers, J. E. M. Haverkort, J. G. Rivas, *Nano Lett.* **2015**, *15*, 4557.
[13] S. Nakamura, M. R. Krames, *Proc. IEEE* **2013**, *101*, 2211.
[14] M.-T. Chen, M.-P. Lu, Y.-J. Wu, J. Song, C.-Y. Lee, M.-Y. Lu, Y.-C. Chang, L.-J. Chou, Z. L. Wang, L.-J. Chen, *Nano Lett.* **2010**, *10*, 4387.
[15] S. Xu, C. Xu, Y. Liu, Y. Hu, R. Yang, Q. Yang, J.-H. Ryou, H. J. Kim, Z. Lochner, S. Choi, R. Dupuis, Z. L. Wang, *Adv. Mater.* **2010**, *22*, 4749.
[16] T. Zhai, X. Fang, L. Li, Y. Bando, D. Golberg, *Nanoscale* **2010**, *2*, 168.
[17] Y. Huang, X. Duan, C. M. Lieber, *Small* **2005**, *1*, 142.
[18] X. Duan, Y. Huang, R. Agarwal, C. M. Lieber, *Nature* **2003**, *421*, 241.
[19] M. Xiaoming, F. Guojia, L. Hao, H. Huihui, L. Songzhan, W. Haoning, Q. Pingli, *Semicond. Sci. Technol.* **2013**, *28*, 015016.
[20] D. V. Esposito, I. Levin, T. P. Moffat, A. A. Talin, *Nat. Mater.* **2013**, *12*, 562.
[21] Q. Wang, A. T. Connie, H. P. T. Nguyen, M. G. Kibria, S. Zhao, S. Sharif, I. Shih, Z. Mi, *Nanotechnology* **2013**, *24*, 345201.
[22] M. Tchernycheva, V. Neplokh, H. Zhang, P. Lavenus, L. Rigutti, F. Bayle, F. H. Julien, A. Babichev, G. Jacopin, L. Largeau, R. Ciechonski, G. Vescovi, O. Kryliouk, *Nanoscale* **2015**, *7*, 11692.
[23] C. Pan, W. Guo, L. Dong, G. Zhu, Z. L. Wang, *Adv. Mater.* **2012**, *24*, 3356.
[24] C. Yang, S. Liu, M. Li, X. Wang, J. Zhu, R. Chong, D. Yang, W.-H. Zhang, C. Li, *J. Colloid Interface Sci.* **2013**, *393*, 58.
[25] X. Mo, G. Fang, H. Long, S. Li, H. Wang, Z. Chen, H. Huang, W. Zeng, Y. Zhang, C. Pan, *Phys. Chem. Chem. Phys.* **2014**, *16*, 9302.
[26] R. Bao, C. Wang, L. Dong, R. Yu, K. Zhao, Z. L. Wang, C. Pan, *Adv. Funct. Mater.* **2015**, *25*, 2884.
[27] P. Chen, X. Ma, D. Yang, *Appl. Phys. Lett.* **2006**, *89*, 111112.
[28] C. Wang, R. Bao, K. Zhao, T. Zhang, L. Dong, C. Pan, *Nano Energy* **2015**, *14*, 364.
[29] P. Elavarthi, A. A. Kumar, G. Murali, D. A. Reddy, K. R. Gunasekhar, *J. Alloys Compd.* **2016**, *656*, 510.
[30] O. Vigil, I. Riech, M. Garcia-Rocha, O. Zelaya-Angel, *J. Vac. Sci. Technol. A* **1997**, *15*, 2282.
[31] J. Aguilar-Hernández, G. Contreras-Puente, A. Morales-Acevedo, O. Vigil-Galán, F. Cruz-Gandarilla, J. Vidal-Larramendi, A. Escamilla-Esquivel, H. Hernández-Contreras, M. Hesiquio-Garduño, A. Arias-Carbajal, M. Chavarría-Castañeda, G. Arriaga-Mejía, *Semicond. Sci. Technol.* **2003**, *18*, 111.
[32] R. Poulomi, S. S. Kumar, *J. Phys. D: Appl. Phys.* **2006**, *39*, 4771.
[33] X. Xu, Y. Zhao, E. J. Sie, Y. Lu, B. Liu, S. A. Ekahana, X. Ju, Q. Jiang, J. Wang, H. Sun, T. C. Sum, C. H. A. Huan, Y. P. Feng, Q. Xiong, *ACS Nano* **2011**, *5*, 3660.
[34] R. H. Bube, *Phys. Rev.* **1955**, *99*, 1105.

Received: May 8, 2016
Revised: July 27, 2016
Published online: